The Final Report

Title: Extremely Low Noise Carbon Nanotubes for Peltier and Photo-detector Device Applications

Principal Investigator: Young Hee Lee, Ph. D.SungKyunKwan University
Telephone: +82-31-299-6507
E-mail: leeyoung@skku.edu

Contract Number: FA4869-07-1-4071

AOARD Reference Number: AOARD-074071

AOARD Program Manager: Sang-ho Byun

Period of Performance: 1 year

Submission Date: 8 Oct. 2008

Report Documentation Page	*Form Approved* *OMB No. 0704-0188*

Public reporting burden for the collection of information is estimated to average 1 hour per response, including the time for reviewing instructions, searching existing data sources, gathering and maintaining the data needed, and completing and reviewing the collection of information. Send comments regarding this burden estimate or any other aspect of this collection of information, including suggestions for reducing this burden, to Washington Headquarters Services, Directorate for Information Operations and Reports, 1215 Jefferson Davis Highway, Suite 1204, Arlington VA 22202-4302. Respondents should be aware that notwithstanding any other provision of law, no person shall be subject to a penalty for failing to comply with a collection of information if it does not display a currently valid OMB control number.

1. REPORT DATE **08 OCT 2008**	2. REPORT TYPE **Final**	3. DATES COVERED **15-06-2007 to 14-06-2008**

4. TITLE AND SUBTITLE **Fundamental Nanoscience for Development of Devices**	5a. CONTRACT NUMBER **FA48690714071**
	5b. GRANT NUMBER
	5c. PROGRAM ELEMENT NUMBER
6. AUTHOR(S) **Sungho Jin; Younghee Lee; Moonho Jo; Sooyoung Park**	5d. PROJECT NUMBER
	5e. TASK NUMBER
	5f. WORK UNIT NUMBER
7. PERFORMING ORGANIZATION NAME(S) AND ADDRESS(ES) **Korea Foundation for International Cooperation of Science & Technology,275-7 Yangjae Dong, Seocho Gu,Seoul,South Korea,NA,NA**	8. PERFORMING ORGANIZATION REPORT NUMBER **N/A**
9. SPONSORING/MONITORING AGENCY NAME(S) AND ADDRESS(ES) **AOARD, UNIT 45002, APO, AP, 96337-5002**	10. SPONSOR/MONITOR'S ACRONYM(S) **AOARD**
	11. SPONSOR/MONITOR'S REPORT NUMBER(S) **AOARD-074071**

12. DISTRIBUTION/AVAILABILITY STATEMENT

Approved for public release; distribution unlimited

13. SUPPLEMENTARY NOTES

14. ABSTRACT

The report contains final reports from four separate projects co-funded by AFOSR/AOARD and Korean MEST. The four projects were 1) High-Resolution, Larger-Area Nanoimprint Lithography Using Crystalline Lattice Images and Electron-Emitting Nanoprobes; 2) Extremely Low Noise Carbon Nanotubes for Peltier and Photo-detector Device Applications; 3) SiGe Alloy Nanowire Photonics; and 4) Self-Assembled Liquid Crystalline Gels: From Nanosructure to Function.

15. SUBJECT TERMS

16. SECURITY CLASSIFICATION OF:			17. LIMITATION OF ABSTRACT	18. NUMBER OF PAGES	19a. NAME OF RESPONSIBLE PERSON
a. REPORT **unclassified**	b. ABSTRACT **unclassified**	c. THIS PAGE **unclassified**	**Same as Report (SAR)**	**39**	

NBIT PROGRAM 2007

Report

Part I. General Information

		For KOSEF use only	
1. Project Title (in English): Extremely Low Noise Carbon Nanotubes for Peltier and Photo-detector Device Applications (in Korean):			
2. Research Code Number	200702	3. Sub-research field	nanophysics
4. Research Duration	From 20070401 To 20080331		

5. Applicant Information

Korean Principal Investigator (KPI)		US Principal Investigator (USPI)	
Full Name (age)	Young Hee Lee (52)	Full Name (age)	Moon J. Kim (45)
Nationality	Korea	Nationality	Korea
Affiliation (department)	Sungkyunkwan University (Department of Physics)	Affiliation (department)	University of Texas at Dallas (Department of Electrical Engineering)
Position	Professor	Position	Professor
Telephone	+82-31-299-6507	Telephone	+001-972-883-6635
Fax	+82-31-290-5954	Fax	+001-972-883-6629
E-mail	leeyoung@skku.edu	E-mail	moonkim@utdallas.edu
Address	440-746, 300 Cheoncheon-dong, Jangan-gu, Suwon, Korea	Address	EC 33, Box 830688 Richardson, Texas 75083-0688, U.S.A.

6. Authentication and Commitment

Korean Principal Investigator (KPI)

Name Young Hee Lee Date 2008.10.06

MID-TERM REPORT

Task: Extremely Low Noise Carbon Nanotubes for Peltier and Photo-detector Device Applications

Korea Principal Investigator: Young Hee Lee, Ph. D.
SungKyunKwan University

U.S. Principal Investigators: Moon J. Kim, Ph. D.
University of Texas at Dallas
Minhee Yun, Ph. D.
University of Pittsburgh

Report Period; April 07 to March 08

I. Progress Summary

1. Controlled carbon nanotubes (CNTs) with single-wall and multi-wall and larger than 10μm have been successfully grown by chemical vapor deposition (CVD) method
2. Various contact electrodes including Pd, Hf, Ag, Ti, Cr, and Au have been fabricated for the investigation of Schottky barriers
3. Single CNT field-effect transistors (FET) have been successfully fabricated and are under investigating
4. Optoelectronic properties of CdSe quantum dot (QD)-embedded CNT-FET has been investigated
5. Korea PI and his research students visited US partner in order to provide and exchange high quality international research experiences
6. 4 journal papers have been published or accepted for publication

II. Significant Technical Progress at SungKyunKwan University

II-A Fabrication of various metals/CNT contact

The CNT devices are fabricated on n-doped silicon substrate with 400 nm of thermally grown oxide. Prior to CNT growth, Cr/Au lead lines and contact pads are deposited for easier location and fabrication of FET structures. These are fabricated by an optical lithography deposition and liftoff process. Nanotubes were grown by thermal CVD at 900 °C during about 20 min, using a gas mixture of hydrogen and methane under atmospheric pressure.

After fabrication of devices (See US team update for details), CNT devices are tested in ambient room conditions as well as in a closed-cycle refrigerator capable of stable and controlled temperatures from 20 Kelvin to 300 Kelvin. The results of testing at low temperatures are imperative for the study of electrical transport properties of the device since other methods such as capacitance/voltage testing require data (such as electrically active area) that is unknown for CNT.

Figure 1 (b) shows the I-V characteristics with respect to four different electrodes (Cr1, Ni, Mo-Ni, and Cr2) on the same SWCNT at 30 K and 295 K with V_{gs} = 0 V. For all metals utilized on this nanotube, I-V characteristics showed clear temperature dependence, and reduced conduction at low temperatures. This is primarily due to the reduction of thermally-assisted tunneling and emission. For the Ni device, analysis of the differential conductance yielded contact resistances from 3.94 MΩ (295 K) to 94 GΩ (~30 K). The Schottky barrier height was around 40.5 meV. Another unique device analyzed was a hybrid Mo-Ni FET structure. Although the channel length of this device was over a micron long (contrary to the 400 nm length of other devices shown in figure 1 (a)), the device had similar I-V characteristics to the Ni-only FET structure. This is due to electron transport being almost completely dependent on the contacts in this case, not the nanotube. Transport characteristics were also consistent with the presence of a Schottky barrier at the source-nanotube interface. Contact resistance of this device decreased pronouncedly for lower temperatures, achieving a low of 3.95 MΩ at 295 K and an insulator-like 280 GΩ, at 30 K. The large increase in resistance compared to other devices is partially due to the longer channel length – where acoustic phonon scattering could be significant and does not disappear, even at low temperatures. The barrier height is estimated at 41 meV at the source-nanotube junction corresponding to the Mo electrode.

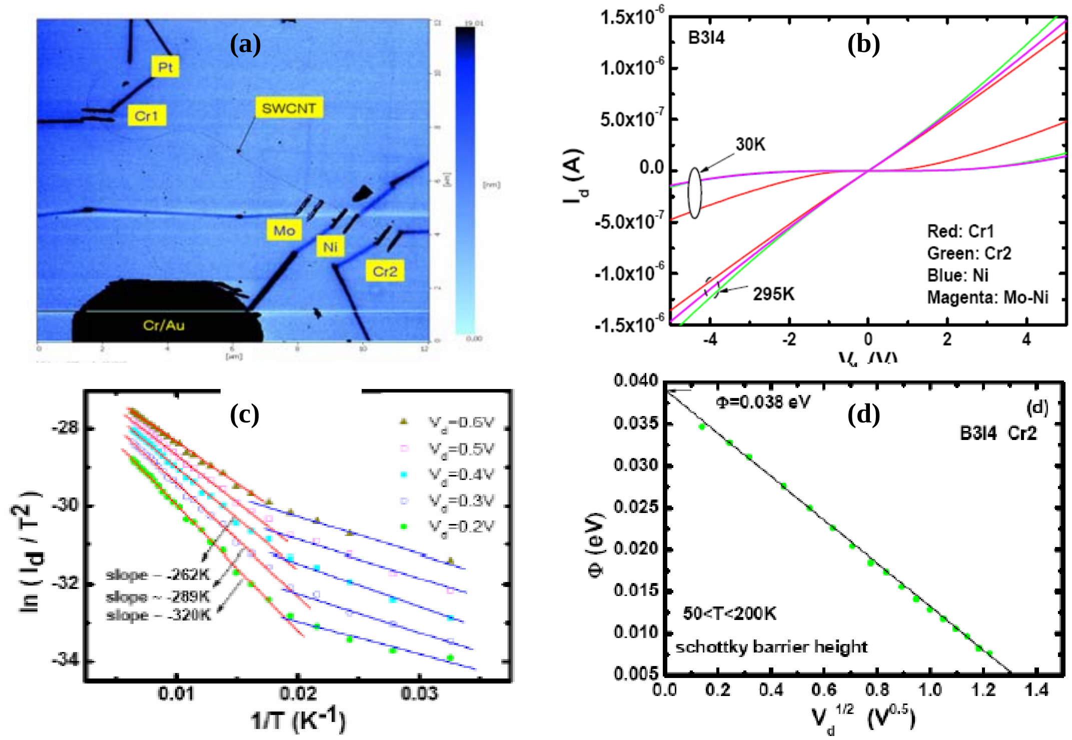

Figure 1. (a) Various contact electrodes by AFM image, I-V characteristics (b to d) of SWCNT-FET by various

In Figure 1 (c-d), barrier height calculations for the Cr1 electrode are shown. Due to the best fitting to the Schottky model of conduction, we have confirmed the existence of Schottky barriers at the nanotube-drain and nanotube-source electrodes. After a comprehensive temperature dependence analysis, the device behaved according to the Schottky model of electron transport in equation 1. I-V measurements for Cr1 device at temperatures ranging from 30 K to 295 K yielded a Schottky model - I_d~T correlation. The Cr1 device displayed Schottky behavior with a barrier height of 38 meV. Once again indicating thermionic emission and thermally assisted tunneling dominating the total current of this device. The piecewise linear representation of the data utilizes best-fit lines according to the Schottky model of carrier transport $I \propto T^2 \cdot \exp\left(-\frac{e\Phi_e}{kT}\right)$ (Equation1). Due to the strong correlation with this model, the barrier height could be estimated by $\Phi_e \propto \Phi_b - \left(\frac{eV}{\pi\varepsilon_i\varepsilon_0}\right)^{1/2}$ (Equation 2) where ϕ_b is derived from the best fit line of measured barrier height for more than 20 values of V (V_{ds}). We have, using an e-beam and focused ion beam method, fabricated CNT-FET structures with a SiO_2 back gate. The nanotube-electrode Schottky barriers were expected when utilizing a semiconducting single-walled carbon nanotube. Further exploration into the Poole-Frenkel phenomenon found in the Cr2 device will be needed to determine more precisely the rational for this mechanism in a CNT-FET. FET characteristics are not available from this sample due to leakage in the oxide. The 400 – 500 nm of SiO_2 was grown thermally, but seemed to have been damaged during CNT growth. To further compare performance of different metals as contacts to nanotubes, more devices will be required utilizing an all e-beam method to eliminate the risk of FIB leakage current. Improved silicon dioxide along with other gate dielectrics will also be utilized in the future to prevent oxide leakage and include FET characteristics.

II-B. Optoelectronic properties of CdSe quantum dot/CNT FET:

CdSe quantum dots have been decorated on single-walled carbon nanotubes (SWCNTs) by combining a method of chemical modification of substrate with a gate-bias control. CdSe/ZnS core/shell quantum dots were negatively charged by adding mercaptoacetic acid(MAA). The silicon oxide substrate was decorated by octadecyltrichlorosilane (OTS) and converted to hydrophobic surface. The negatively charged CdSe quantum dots were adsorbed on the SWCNT surface by applying a negative gate bias. The selective adsorption of CdSe quantum dots on SWCNTs was confirmed by confocal microscopy. As shown in Figure 2, the measured photocurrent clearly demonstrates that CdSe quantum-dot decorated SWCNT can be used for photodetection and solar cells that are operable over a wide range of wavelengths.

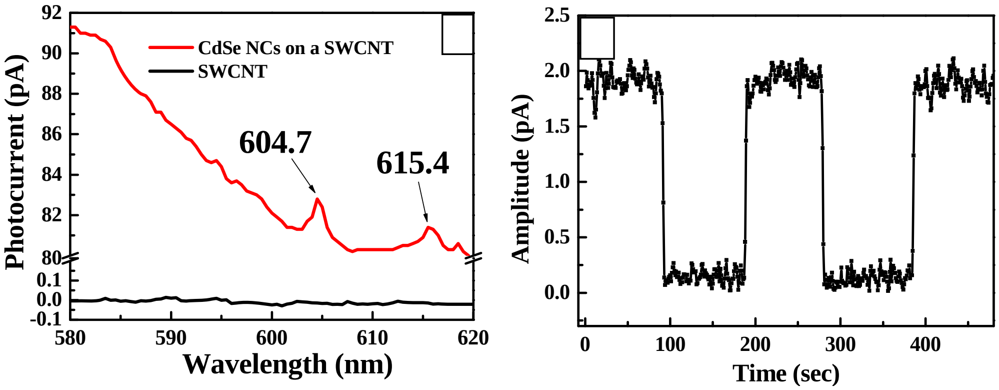

Figure 2. Measurements of photocurrents based on wavelength and operation time

III. Significant Technical Progress at University of Pittsburgh and University of Texas at Dallas

Samples received from the Korean team contain grown CNT with various alignment markers and in many cases - large contact pads. For the creation of devices, two different methods have been utilized– an all e-beam method (method 1), and a hybrid e-beam and focused ion beam (FIB) deposition method (method 2). For the first method, Ti/Au lead lines are fabricated from large contact pads to locations near AFM-identified nanotubes first so that shorter (More precisely located) lead lines for each individual metal can be used to create small source and drain electrodes. The fabrication process consists of photoresist deposition, electron beam lithography, and electron beam evaporation (or Sputtering in case of Mo) of each metal. Each electrode metal was patterned separately in this manner. For each of the metal types, ~15-30 nm of metal was deposited by e-beam lithography in sub -5x10^{-7} torr vacuum. An example of this is found in Figure 3 (a).

For fabrication method 2, the small electrodes of each metal are patterned first and this is followed by a FIB Pt lead line deposition to connect these 0.1 μm by 1 μm electrodes to large probable contact pads. The FIB current was reduced to 3 eV in an attempt to reduce beam current and scattering to prevent damage to the nanotube. It has been found that at such a voltage, nanotube etching occurred very slowly and hence the risk of damage was significantly reduced. Also, it should be noted that the lead lines are large enough so that the resistance of each is negligible (a few hundred ohms or less) compared to the contact resistance and even CNT resistance. All other procedures described for the all e-beam method are the same as for method 1.

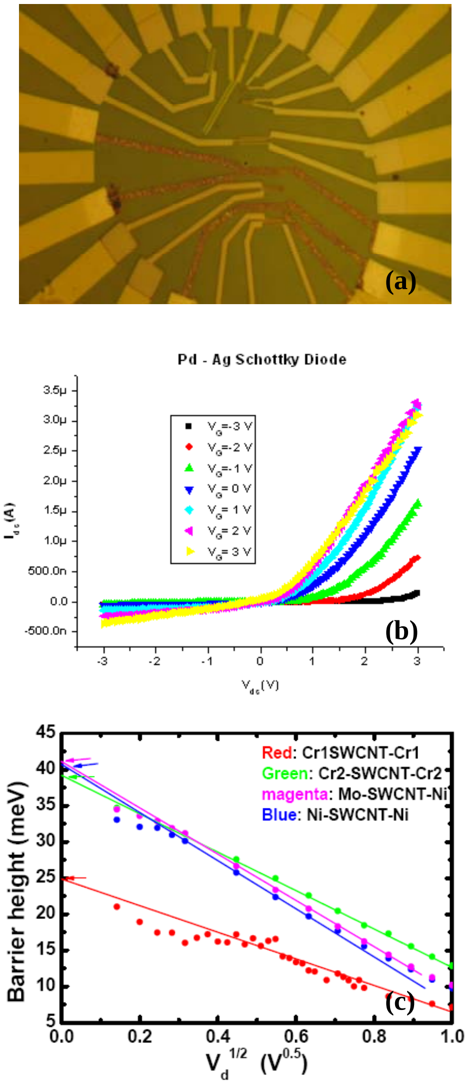

Figure 3. (a) Contact electrodes on the top of the SWCNT, (b) I-V characteristics of Pd-Ag electrode, and (c) Schottky barrier heights based on Cr, Mo, and Ni electrodes.

Utilizing e-beam lithography, devices have been fabricated with slightly different parameters to produce the most consistent and successful results. It has been found that device success rates are far better and possibly more consistent when CNT are not exposed to an electron beam (as in SEM imaging) prior to fabrication and testing. It is also believed that photoresist scum can drastically change current and voltage statistics due to the nature of the nanometer size scale of carbon nanotubes. With this in mind, fabrication has been altered so that lower (≤ 10 keV) SEM acceleration voltages, as well as low currents (≤ ~200 pA) are utilized during e-beam exposures in the fabrication of CNT source and drain electrodes. Multi-step resist processes with larger undercut structures to enable easier liftoff have also been utilized to allow for easier liftoff and less possible stress during processing.

Devices fabricated utilizing all e-beam lithography to generate lead lines and electrodes have thus far exhibited much better conduction properties. It is, however, not clear whether this is due to the larger amount of such devices produced or if there is a correlation between FIB-CNT damage caused from stray Ag and Pt atoms striking the CNT (This was avoided). Although not necessarily a factor in changing the Schottky barrier properties, using all e-beam lithography has led to the improvement of overall device performance. For the generated Schottky devices based upon Ni, Cr, and Mo metals, symmetric I-V characteristics were generated even when hybrid devices were examined. When the situation is changed further – so that the work functions of metals are much different, as shown in figure 3 (b), Schottky diode devices can be fabricated. In this device, Pd and Ag electrodes were utilized to effectively create a Schottky diode. At negative V_{ds} the device exhibits extremely low conductance due to the high barrier height at the Ag – nanotube interface preventing the injection of carriers into the valence band of the CNT. This barrier height is estimated at ~83 meV using curve fitting to a Schottky diode model. The positive V_{ds} potentials, however, show very small near –ohmic behavior and thus much greater current densities. This side is indicative of the Pd electrode contact. This device shows a diode threshold voltage of ~ 1V. A Zener-like breakdown is not shown since at high negative V_{ds} leakage current becomes more prominent due to the already low current through the Ag – CNT contact (few nanoamps at V_{GS} = 0).

Figure 3 (c) shows barrier height data for four devices based on the FIB lead line method. For the Cr1, Ni, and Mo-Ni devices the barrier height was found utilizing the Schottky model and sufficiently describes conduction from 50 K to 200 K. The Cr2 device utilized the same relationship for barrier height, but exhibited Pool-Frenkel type transport for 50 K to 100 K as opposed to the basic Schottky model. Not enough devices have been analyzed yet to create a formal comparison of barrier heights, while using a reference metal (typically Pd due to ease of evaporation and good I-V characteristics), from devices present on the same, as well as different nanotubes. The current trend yields barrier height in order: Pd < Cr < Ni, Mo < Ag. Note that figure 3 (c) presents some of the data gathered regarding Schottky barrier height measurements. The work functions of these materials are in the opposite (descending) order, as was expected for a better line-up of the metal fermi level with the CNT valence band. The data set is not statistically relevant, and not all comparable (lack of reference in some cases thus far), therefore it is imperative to use multiple devices with the same metals to begin extracting useful trends. All current and future devices fabricated will contain multiple reference electrodes, to ensure better success in comparing data.

IV. Publications

Formatted: Bullets and Numbering

1. S. Y. Jeong et al. Chirality-specific transport phenomena of isolated singlewalled carbon nanotube, Phys. Stat. Sol. B 244, 4204 (07).
2. Seung Yol Jeong, Seong Chu Lim, Dong Jae Bae, Young Hee Lee, Hyun Jin Shin, Seon-Mi Yoon, Jae Young Choi, Ok Hwan Cha, Mun Seok Jeong, David Perello, and Minhee Yun, "Photocurrent of CdSe nanocrystals on singlewalled carbon nanotube-field effect transistor", Appl. Phys. Lett., 92(24), 243103-1~243103-3, (Jun. 16, 2008.)
3. Seung Yol Jeong, Sang Hyun Jeon, Gang Hee Han, Kay Hyeok An, Dong Jae Bae, Seong Chu Lim, Ha Ryong Hwang, Chang Soo Han, and Young Hee Lee, 'Efficient Synthesis of Individual Single-Walled Carbon Nanotube by Water-Based Catalyst with Poly(vinylpyrrolidone)', Journal of Nanoscience and nanotechnology, 8(1), 329-334 , (Jan. 2008.)
4. David Perello et. al., “Schottky Barrier Engineering in Carbon Nanotube with Various Metal Electrodes”, Preoceedings of Nanotechnology 2007, 7th IEEE-NANO, Hong Kong
5. Innam Lee, Ho Il park, Seongyong Park, Moon J. Kim, and Minhee Yun, “Highly Reproducible Single Polymer Nanowires using Electrophoresis Method”, Nano, 3(2) 75-85 (2008)
6. Woo Jong Yu, Seung Yol Jeong, Ki Kang Kim, Bo Ram Kang, Dong Jae Bae, Min Baek Lee, Seung Hun Hong, Sunanda Prabhu Gaunkar, Didier Pribat, David Perello, Minhee Yun, Jae-Young Choi, and Young Hee Lee, ‘Bias-induced doping engineering with ionic adsorbates on singlewalled carbon nanotube thin film transistor’, accepted to New J. Phys. (2008)

V. Future Plan

Our approach to fabricate several different metal electrodes on the same CNTs has been progress. The fitting model for instance, Schottky model and Poole-Frenkel model has been searched to determine the Schottky barrier. This will soon be completed. A strategy to increase the adsorption of quantum dots such as Si and CdSe has been designed and implemented for fabrication of photodetector that are operable at visible range by the end of second year. We will also invent a new design of n/p doping Iby using dopants that are stable in air. Of particular interest is an n-type doping. Our preliminary results show that stable n-doping principle on CNTs can be constructed. Using this idea, n/p junction will be constructed and optoelectronic photodetector will be tested and compared to the QD-decorated ones.

Parallel to fabrication process, the chirality and diameter of SWCNTs will be identified by utilizing Confocal Raman spectroscopy. This aids in non-destructive (and in-situ) characterization of the devices. The photo response will be also measured via photocurrent measurement with light illumination by a spectrum of wavelengths. The electronic-structure related photocurrent resonance will be also searched during this measurement, particularly at low temperature.

The Final Report

Title: **"SiGe Alloy Nanowire Photonics"**

Principal Investigator:

Prof. Moon-Ho Jo, Department of Materials Science and Engineering, POSTECH, Korea

Telephone: +81-54-279-2158

Facsimile: +81-3-5410-4407

E-mail: mhjo@postech.ac.kr

Contract Number: FA4869-07-1-4071

AOARD Reference Number: AOARD-074071

AOARD **Program Manager:** Sang-ho Byun

Period of Performance: 1 year

Submission Date: 8 Oct 2008

Progress Report, Final-Term:
"SiGe Alloy Nanowire Photonics"

October 6 2008

Principal Investigators:

- Korean PI: Prof. Moon-Ho Jo, Department of Materials Science and Engineering, POSTECH, Korea
- US PI: Prof. Hongkun Park, Department of Chemistry and Chemical Biology, Harvard University, United States

Research Achievements:

1. Growth and doping of $Si_{1-x}Ge_x$ nanowires for the unit optical components:

- Journal Article: *Applied Physics Letters* **91**, 033104 (2007): "Fabrication of $Si_{1-x}Ge_x$ alloy nanowire field-effect transistors" by Cheol-Joo Kim, Won-Hwa Park, Jee-Eun Yang, Hyun-Seung Lee, Sunglyul Maeng, Zee Hwan Kim, Hyun M. Jang and **Moon-Ho Jo**

- Summary: We present the demonstration of nanowire field-effect transistors incorporating group IV alloy nanowires, $Si_{1-x}Ge_x$. Single-crystalline $Si_{1-x}Ge_x$ alloy nanowires were grown by a Au catalyst-assisted chemical vapor synthesis using SiH_4 and GeH_4 precursors, and the alloy composition was reproducibly controlled in the whole composition range by controlling the kinetics of catalytic decomposition of precursors. Complementary *in situ* doping of $Si_{1-x}Ge_x$ nanowires was achieved by PH_3 and B_2H_6 incorporation during the synthesis for *n*- and *p*-type field-effect transistors. The availability of both *n*- and *p*-type $Si_{1-x}Ge_x$ nanowire circuit components suggests implications for group IV semiconductor nanowire electronics and optoelectronics.

2. Growth of metallic nanowires for the optical device application (field-emission displays):

- Journal Article: *Advanced Materials* **19** 3637 (2007), "Spontaneous chemical vapor growth of NiSi nanowires and their metallic properties", Cheol-Joo Kim, Kibum Kang, Yun Sung Woo, Kyung-Guk Ryu, Heesung Moon, Jae-Myung Kim, Dong-Sik Zang and **Moon-Ho Jo**.

- Summary: We reported a simple and controlled synthesis at low temperatures of where single-crystalline NiSi nanowires by SiH_4 chemical vapor deposition (CVD) on Ni thin films predeposited on various substrates, such as SiO_2/Si, quartz, and indium tin oxide (ITO) substrates. The dimensionality of the Ni-silicides have been reproducibly directed from thin films to single-crystalline nanowires, as well as their phases, by fine-tuning of growth parameters during CVD of a SiH_4 gas precursor on predeposited Ni thin films. Single crystalline NiSi nanowires in this study exhibit typical metallic behaviors, and show promising field-emission properties. It is suggested that our simple method to spontaneously grow NiSi nanowires at low temperatures can provide a practical strategy to fabricate metallic nanostructures based on bottom-up synthetic approaches.

3. Characterizations of individual $Si_{1-x}Ge_x$ nanowires:

- Journal Article: *Applied Physics Letters* **91**, 223107 (2007): "Soild-phase epitaxy of amorphous Si using single-crystalline Si nanowire templates", Yun Sung Woo, Kibum Kang, Jong-Myeong Jeon, **Miyoung Kim** and **Moon-Ho Jo.**

- Summary: We report solid-phase epitaxy of amorphous Si *a*-Si shells using crystalline Si *c*-Si nanowire cores as seed templates. The *c*-Si core/*a*-Si shell nanowire heterostructures were *in situ* synthesized via a two-step chemical vapor deposition: the Au-catalytic decomposition of SiH4 for the core *c*-Si nanowires and the subsequent homogeneous decomposition of SiH4 at higher temperatures for the *a*-Si shells. Upon thermal annealing above 600 °C, the *a*-Si shells crystallize into *c*-Si shells from *c*-Si core nanowires in an epitaxial fashion. We discuss the crystallization kinetics of *a*-Si shells within the frame of Gibbs-Thomson effects arising from the finite size of nanowire seeds.

4. Growth and characterization of metallic nanowires for the optical device application (field-emission displays):

- Journal Article: *Nano Letters* **8** 431 (2008): "The Role of NiO Overlayers on Spontaneous Growth of $NiSi_x$ Nanowires from Ni Seed Layers", Kibum Kang, Sungkyu Kim, Cheol-Joo Kim, and **Moon-Ho Jo.**
- Summary: We report a controllably reproducible and spontaneous growth of single-crystalline $NiSi_x$ nanowires using NiO_x/Ni seed layers during SiH_4 chemical vapor deposition (CVD). We provide evidence that upon the reactions of SiH_4 (vapor)-Ni seed layers (solid), the presence of the NiO_x overlayer on Ni seed layers plays the key role to promote the spontaneous one-dimensional growth of $NiSi_x$ single crystals without employing catalytic nanocrystals. Specifically, the spontaneous nanowire formation on the NiO_x overlayer is understood within the frame of the SiH_4 vapor-phase reaction with out-diffused Ni from the Ni underlayers, where the Ni diffusion is controlled by the NiO_x overlayers for the limited nucleation. We show that single-crystalline $NiSi_x$ nanowires by this self-organized fashion in our synthesis display a narrow diameter distribution, and their average length is set by the thickness of the Ni seed layers. We argue that our simple CVD method employing the bilayers of transition metal and their oxides as the seed layers can provide implication as the general synthetic route for the spontaneous growth of metal-silicide nanowires in large scales**.**

5. Growth and characterization of axially composition modulated $Si_{1-x}Ge_x$ nanowires for the unit optical components:

- Journal Article: *Applied Physics Letters* **92**, 263111 (2008): "Axially graded heteroepitaxy and Raman spectroscopic characterizations of $Si_{1-x}Ge_x$ nanowires", Jee-Eun Yang, Won-Hwa Park, Cheol-Joo Kim, Zee Hwan Kim, and **Moon-Ho Jo.**
- Summary: We report the axially graded heteroepitaxy of $Si_{1-x}Ge_x$ nanowires, by the kinetic controls of the Au-catalytic decomposition of precursors during chemical vapor syntheses. Transmission electron microscope studies demonstrate that the relative composition of Si and Ge is continuously graded along the uniformly thick nanowires, sharing the same crystal structures with the continuously varying lattices. We also employed a confocal Raman scattering imaging technique, and showed that the local variations in Raman phonon bands, specific to Si and Ge alloying ($\nu_{Si–Si}$, $\nu_{Si–Ge}$, and $\nu_{Ge–Ge}$) can be spatially and spectrally resolved along the individual nanowires, within the spatial resolution of ~500 nm.

6. Large area growth of Ge nanowires:

- Journal Article: *Advanced Materials* Accepted for Publication (2008): "Low-Temperature Deterministic Growth of Ge Nanowires Using Cu Solid-Catalysts", Kibum Kang, Dong-An Kim, Hyun-Seung Lee, Cheol-Joo Kim, Jee-Eun Yang and **Moon-Ho Jo.**
- Summary: We report the low-temperature growth of Ge NWs by using Cu-catalysts at as low as 200 °C in a deterministic manner, so that the diameter of Ge NWs is uniformly distributed at 7 nm, directly templated from the identical size of Cu

catalysts, with the consistent [011] crystallographic orientation. Specifically it was found that the Cu catalyst tips are consistently orthorhombic Cu3Ge with the heteroepitaxial relation with the cubic Ge NWs, as [010]tip//[011]NW, along the wire axes. We attribute the low-temperature growth of 200 °C, which is well below the Cu-Ge eutectic temperature of 644 °C, to the growth by the catalytic decomposition of Ge precursors onto the solid-phase Cu catalysts, and describe distinct manifestations of the solid-catalytic growth from the parallel comparison to the growth from the eutectic liquids catalysts. We further demonstrate that the solid-catalytic growth in our study can be readily adapted for the vertical growth by an epitaxial manner on Si substrates. We argue that the low-temperature growth of semiconductor NWs using the solid catalysts can be generally accessible, provided that the appropriate combination of solid catalysts and semiconductors are thermodynamically available, thus suggest implication for the potential large-area integrated growth on various substrates.

Collaborative Team Efforts:

1. Program kick-off meeting: June 4-5 2007, Seoul Korea by both KPI and USPI

2. Research training of a graduate student (Cheol-Joo Kim from KPI) at the USPI Lab: Jul 19-27 2007

: Collaboratively developed and bench-marked individual nanowire optoelectronic measurement set-ups:

Optoelectronic measurement set-ups

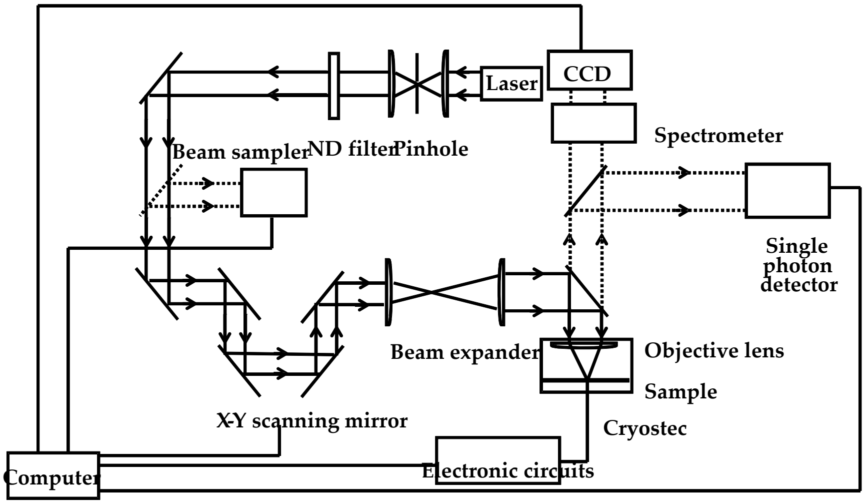

3. The 1st Team Meeting: Jul 19-21 2007, Harvard University, US (KPI-USPI)

4. US researcher (Dr Myung-Han Yoon from USPI) visit to KPI's Lab: Nov 13 2007

5. The 2nd Team Meeting: Dec 4-7 2007, Seoul, Korea (KPI-USPI)

6. Research training of a graduate student (Hyun Seung Lee from KPI) at the USPI Lab: Jun 06 - Sep 07 2008

: Collaboratively characterized photoconductivity of $Si_{1-x}Ge_x$ nanowire devices:

7. The 3rd Team Meeting: Aug 7-8 2008, Seoul, Korea (KPI-USPI)

Team Achievements:

- *Applied Physics Letters* **91**, 223107 (2007): "Solid-phase epitaxy of amorphous Si using single-crystalline Si nanowire templates", Yun Sung Woo, Kibum Kang, Jong-Myeong Jeon, Miyoung Kim and Moon-Ho Jo**.**
- ***2008 Gordon Conference*****,** (July 27 - August 1, 2008 Tilton, NH, US): Plasmonics, Optics At The Nanoscale, "Electrical Detection of Surface Plasmons in the Near Field", Abram L. Falk, Frank H. Koppens, Chun Yu, Nathalie de Leon, Kibum Kang, Moon-Ho Jo, Mikhail Lukin, Hongkun Park
- Article in preparation: "Near-Field Electrical Detection of Guided Surface Plasmons", Abram L. Falk, Frank H. Koppens, Chun Yu, Kibum Kang, Nathalie de Leon , Alexey Akimov, Moon-Ho Jo, Mikhail Lukin, and Hongkun Park

The Final Report

Title: HIGH-RESOLUTION, LARGE-AREA, NANO IMPRINT LITHOGRAPHY USING ELECTRON LATTICE IMAGES AND ELECTRON-EMITTING NANOPROBES

Principal Investigator:
KPI = Prof. Ki-Bum Kim, Seoul National Univ.)

Telephone: +82-2-880-7095
E-mail: kibum@snu.ac.kr

Contract Number: FA4869-07-1-4071

AOARD Reference Number: AOARD-074071

AOARD Program Manager: Sang-ho Byun

Period of Performance: 1 year

Submission Date: 8 Oct 2008

Progress Report

(USPI = Prof. Sungho Jin, UC San Diego, KPI = Prof. Ki-Bum Kim, Seoul National Univ.)

Project Title

HIGH-RESOLUTION, LARGE-AREA, NANO IMPRINT LITHOGRAPHY USING ELECTRON LATTICE IMAGES AND ELECTRON-EMITTING NANOPROBES

The aim of this joint research project (Seoul National University – UC San Diego) is to develop a mold for a large area nano-imprint lithography technique. While there can be many applications, the primary targeting application area is for ultra-high-density, patterned magnetic recording media with the recording density of 1 terabit/in^2, which is about 5 times higher than that of the current hard disk memory in the market. It is generally accepted that such a high recording density requires a patterned media with the recorded magnetic island bit size of ~12.5 nm in diameter.

Prof. Kim's group develops the Si nano pillar array with 1 terabit/in^2 using conventional electron-beam lithography with 100kV and atomic image projection electron-beam lithography. In the e-beam lithography, HSQ is selected as a resist which is known as one of the high-resolution e-beam resists with a patterning capability of less than 10 nm in a low density dot and line patterns. However, the minimum feature size with a high density pattern is still close to or larger than 20 nm. Processing steps for the formation of Si nano-pillar array is composed by e-beam lithography, Si etching by Cl_2 plasma, and strip of remained resist. With the conventional processing scheme, we can successfully fabricate Si nano-pillar array with the pitch size larger than 30 nm as shown in Fig. 1a~1c. However, resist patterns below the 25 nm pitch were not isolated and merged each other due to the e-beam proximity effect. This effect certainly limits the patterning capability which is less than 25 nm. Here, we propose a novel development process of HSQ resist using diluted HF solution in between the conventional TMAH development process, which is called to "two-step development". (The detail fabrication process of Si nano pillar array is explained below this page[1].) Using this method, we can obtain fully isolated resist pattern with pitches from 25 nm down to 15 nm, and the resist pattern with 25 nm pitch was well transferred to the Si substrate (Fig. 1d). The mean diameter and height of them are 20 and 45 nm, respectively. It is also noted that the resist

---

[1] Hydrogen silsesquioxane (HSQ) dissolved in methyl isobutyl ketone (MIBK) was spin-coated on the Si substrate with a thickness of 30 nm and baked at 90 ^oC on a hot plate for 1 min. The HSQ solution (Fox-12) was purchased from Dow Corning. The e-beam exposure was carried out using AIPEL system with 200 keV and a JEOL JBX9300FS with a beam radius of about 2 nm at the accelerating voltage of 100 keV. Dot array patterns of various pitches from 15 nm to 50 nm were exposed with e-beam dose of 1.0 ~ 3.0 mC cm^{-2}. Development was carried out in tetramethylammonium hydroxide (TMAH) 25 % aqueous solution at 21 ^oC for 1 min, followed by rinsing with H_2O for 2 min. Two step development process follows three steps: the first dipping in TMAH solution, the siloxane layer removal step using a dilute hydrofluoric acid (HF) solution (4000:1 DI water:HF), and the second dipping in TMAH solution. The patterned HSQ and Si substrate were etched for 1 min by Cl_2 plasma (operating pressure; 10 mTorr, plasma power; 75 W) using an RF plasma chamber (Oxford plasmalab 80). After dry etching step, residual HSQ was removed by HF dip.

patterns of 20 and 15 nm pitches were not successfully transferred to Si substrate. We believe that this is due to the limitation of plasma etching (anisotropy characteristic of plasma etching), which generates the sidewall profile of etched pattern (insets of Fig. 1),

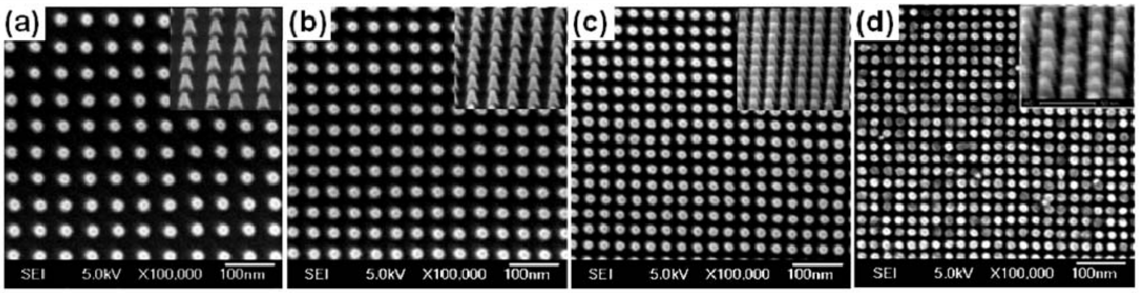

Fig. 1. Plan-view SEM images of the Si nano-pillar array with pitches of (a) 50 nm, (b) 40 nm, (c) 30 nm and (d) 25 nm. The insets are the SEM images tilted view.

The fabricated Si nano-pillar array was sent to Prof. Jin's group (USPI). Figure 2 shows the optical micrograph of the nano-pillar array sample. The magnetic properties of Co/Pd multilayer deposited on the Si nano-pillar array is characterizing in the Prof. Jin's group.

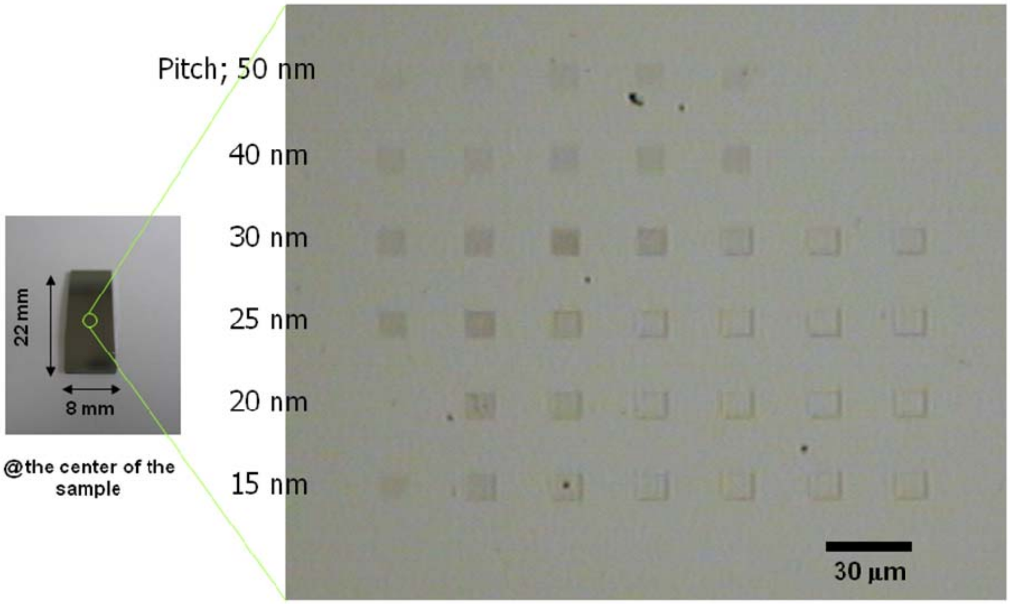

Fig. 2. The optical micrograph image of Si nano-pillar array

Si nano-pillar array is developed using (0001) β-Si_3N_4 mask in AIPEL system. Figure 3 shows the Si nano-pillar array with 150 nm pitch (50nm dot size). We should develop the Si nano-pillar array with 25nm size (below 100 times in AIPEL) for the nano-imprint stamp application.

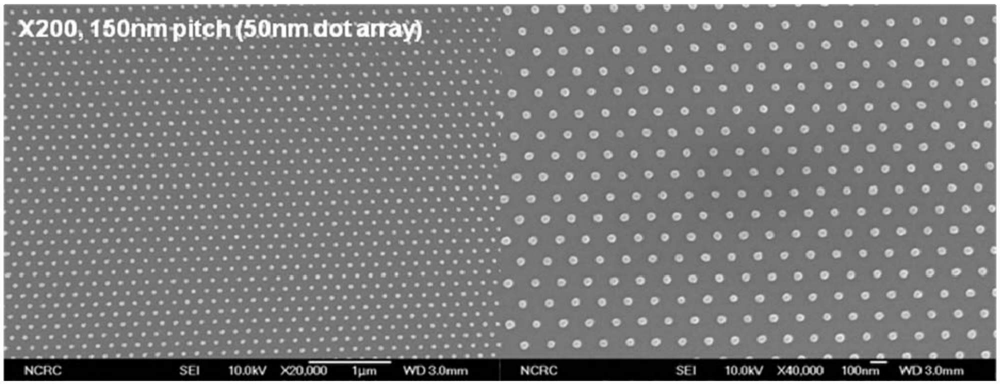

Fig. 3 Si nano-pillar array fabricated by AIPEL. (0001) β-Si_3N_4 was used as a mask. The patterning was performed at 200 times (150nm pitch and 50 nm dot size).

The calixarene e-beam resist which is reported to have a high resolution for e-beam lithography was examined as high energy e-beam lithography. Figure 4 shows the contrast curve data for the calixarene resist in the AIPEL system. The sensitivity of calixarene resist is 10 times higher than that of HSQ resist previous used.

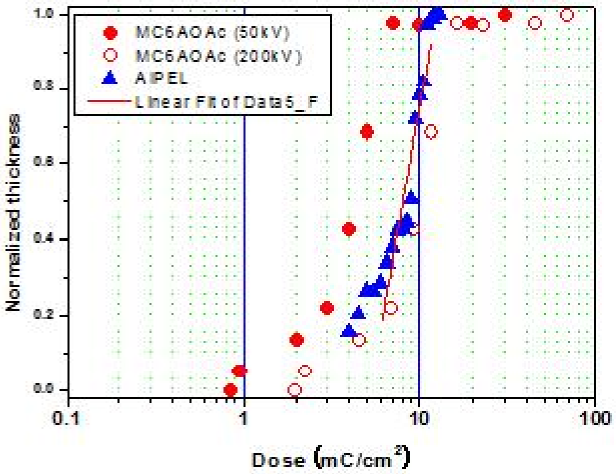

Fig. 4. the contrast curve of calixarene resist (red solid circle: reported data, red open circle: data calculated from reported data, blue solid triangle: AIPEL data)

One of the current issues in the technical field of patterned magnetic media is the problem of magnetic switching field distribution (SFD). To operate the magnetic hard disk drive memory, the recorded bits need to be switched between "1" vs "0" (which is typically obtained by changing of magnetization directions through north pole - south pole switching. The desired magnetic field for switching of recorded bits in future high-density hard disk drive is typically ~5 – 10 KOe. Recent literatures report a substantial undesirable variation of the magnetic switching field when the size of the magnetic nano islands is reduced to below ~ 50 nm. The switching field distribution is sometimes more than 30% from the median coercive force value, which is unacceptable from the hard disk memory application point of view.

Therefore an understanding of why such a switching field variation occurs when the magnetic media becomes nanoscale in dimension, and how to prevent such a phenomenon are of paramount issue that has to be resolved for developing the ultra-high-density magnetic recording media so that the switching of bit information is carried out in a reproducible manner.

The explanations offered so far for the switching field variation phenomenon include;

- Lithographic variations
- Islands sizes variations
- islands edge effects
- Distribution of intrinsic magnetic anisotropy
- Grain orientation and sizes
- Grain boundary variations
- Local compositional variation of Co and Pd at interfaces

While some of the recent literature report that the distribution of intrinsic magnetic anisotropy might be the cause for the switching field variation, there are additional possibilities for the cause of the SFD (switching field distribution) that have not been addressed. One of these possibilities include the fact that the shape of nano-magnet islands fabricated by e-beam lithography is not always uniform. Depending on the shape of the substrate Si pillars (vertical, positively tapered, or negatively tapered) as illustrated in Fig. 5, there can be some sidewall deposition of magnetic recording media, which can contribute to the observed SFD.

Fig. 5. Schematic illustration of undesirable sidewall deposition of magnetic recording media for vertical or positively tapered nano-pillar structure.

Magnetic layer deposition on top of protruding pillars tends to have some corner and sidewall deposition, which will have different magnetic properties and switching fields, and may be one of the sources of SFD in the magnetic islands.

To investigate if removal of such sidewall deposition reduces the SFD problem, we modified the RIE parameters to intentionally alter the shape of the sidewall in Si nanopillars and introduced negative tapered Si column geometry as illustrated in Fig. 6.

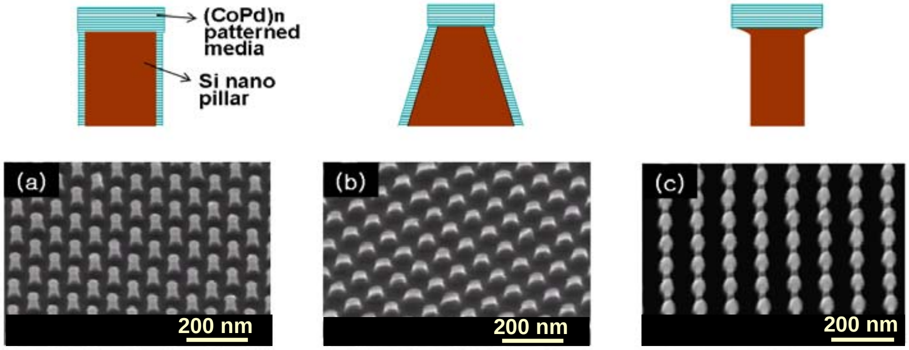

Fig. 6. Control of Si pillar sidewall configurations.

Shown in Figure 7(a)-(c) are example Si pillar patterns with ~30-50 nm diameter having the three different sidewall configurations, fabricated by e-beam lithography utilizing various RIE conditions. Magnetic recording media deposition by sputtering on the pillar top is in progress. Measurements of magnetic M-H loops using advanced, ultra-high-resolution MFM probes (currently being developed at the Jin laboratory) and magneto-optical Kerr effect facilities are in also progress, and will be reported in future progress reports. Finer-scale patterned magnetic island structures are also being developed in collaboration with the KPI's team.

The project requires R&D in both nanostamp fabrication and nano-imprint processes. With regard to these aspects, initial experiments were carried out to begin to establish nano-imprint processes. Using UV-curable elastomer (PDMS) resist as the basis, silicon nanostamps were imprinted onto the resist which was spin coated on a transparent substrate (flat glass or quartz) and UV light was illuminated from underneath to cure the resist during the stamping. The procedure is schematically illustrated in Fig. 8.

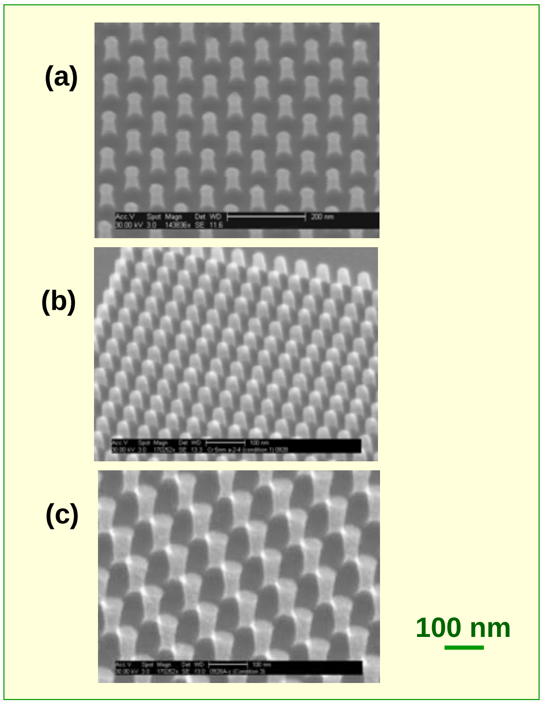

Fig. 7. Different geometry Si nano pillars for magnetic recording media deposition, fabricated by e-beam lithography. (a) vertical sidewall, (b) positively tapered sidewall, (c) negatively tapered sidewall.

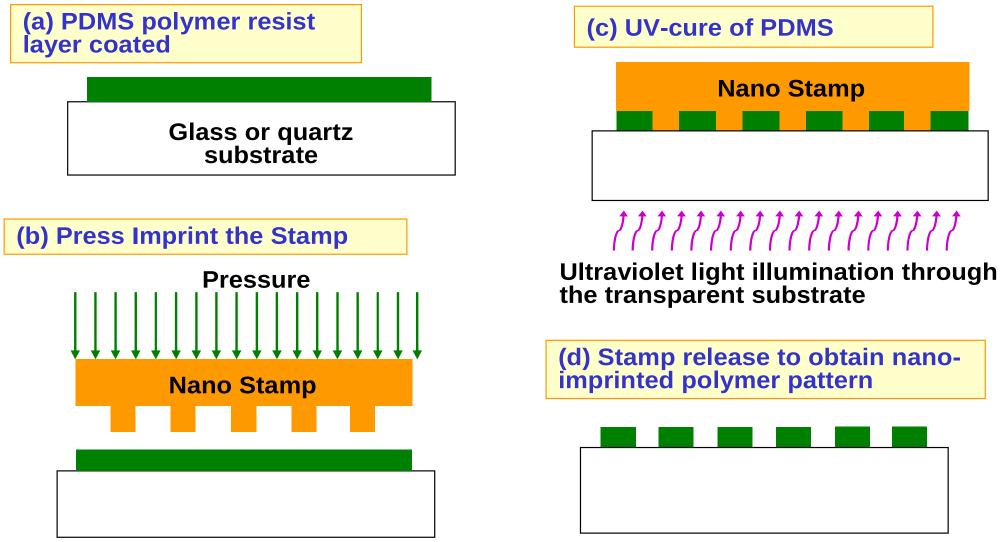

Fig. 8. Schematic illustration of the nano-imprint patterning technique.

Shown in Fig. 9(a) is a SEM micrograph of a line pattern Si imprint stamp (or a mould). The imprinted pattern on the UV-curable resist (Fig. 9(b)) is then examined after the mold (nanostamp) is removed from the resist layer. Circular hole patterns are also fabricated by the nano-imprint process, with 200 nm diameter and 40 nm diameter patterns of the UV-curable PDMS resist shown in Fig. 10(a) and (b), respectively.

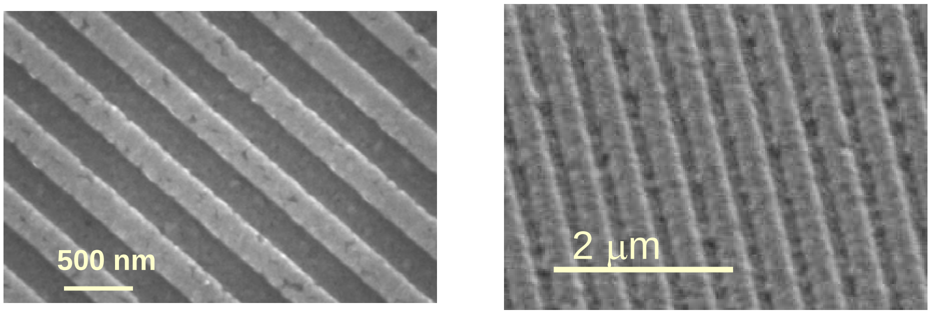
(a) Si stamp with 200 nm lines **(b) Imprinted UV-curable elastomer**

Fig. 9. (a) SEM micrograph of a line-pattern Si imprint stamp, (b) imprinted pattern on the UV-curable resist. .

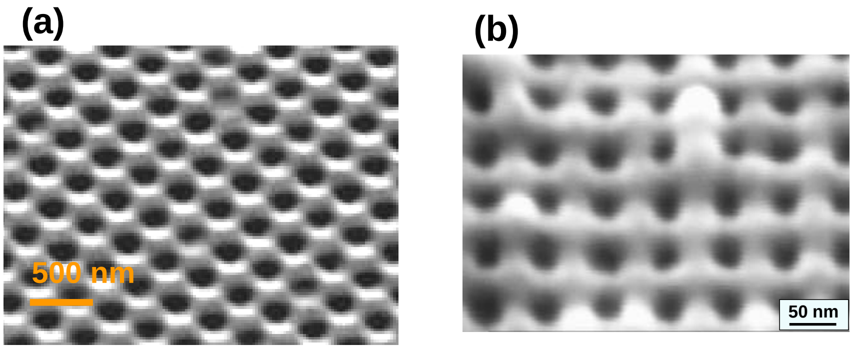

Fig. 10. Circular hole patterns by nano-imprint lithography. (a) 200 nm diameter and (b) 40 nm diameter patterns of the UV-curable PDMS resist.

For study of magnetic island size-dependence of magnetic switching field, distributed magnetic island sizes are sometimes desirable. The question that arises is then how one might be able to make the nano-islands with an intentional distribution of magnetic nano-island sizes. In this study, break-up and spheroidization of thin film layer has been utilized as described below.

As the sample preparation by e-beam lithography is slow and costly, distributed nano island dots with various sizes with a large coverage area (several millimeter area) have been fabricated by sputter deposition of Ni metal film (~3 nm thickness) on Si, followed by annealing heat treatment to break-up and ball up the film into a distributed particle sizes which can serve as etch mask for underlying Si substrate. The Si pattern so obtained is then used as the basis on which a magnetic recording media material of (coPd)n multilayer. This process is schematically illustrated in Fig. 11.

Fabrication for distributed magnetic islands

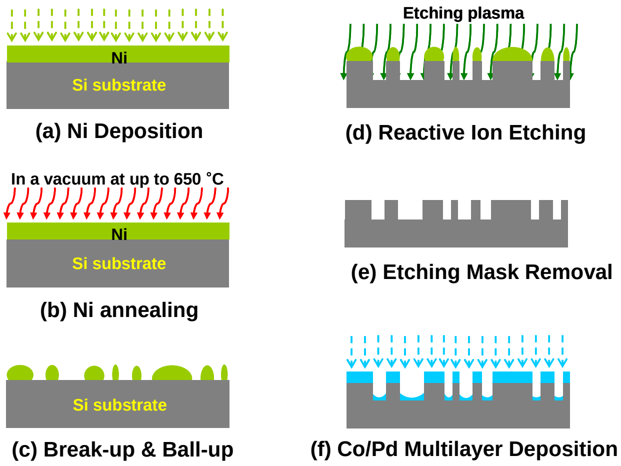

Fig. 11. Fabrication process to obtain magnetic island sizes using balled-up Ni islands as etch mask.

The morphology and size distribution of the Ni islands on Si surface are given in Fig. 12 and Fig. 13. When the thickness of the initial Ni film is increased, the average diameter and the distribution range of island sizes also increase as indicated in Fig. 14.

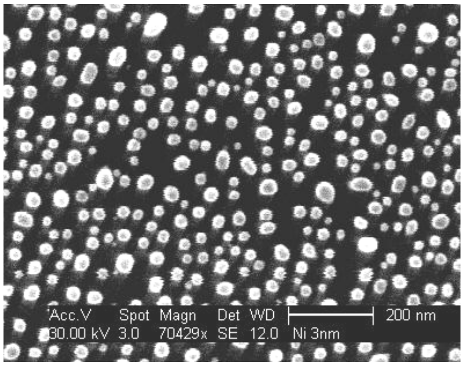

Fig. 12. Distributed size of Ni etch mask islands on Si substrate.

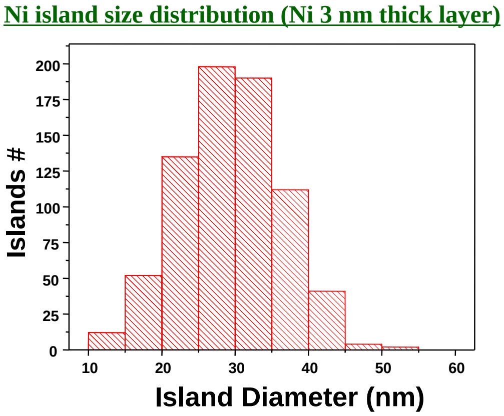

Fig. 13. Ni island particle size distribution.

The nanopatterning of Si underneath the Ni mask islands was carried out by RIE etching of Si. The resultant microstructure is shown in Fig. 15. Vertically aligned Si nanowires (pillars) with distributed diameters are obtained. The Ni islands are etched away by dilute acid, and then high-coercivity magnetic recording media, $(CoPd)_8$ multilayer was deposited with Ta and Pd seed layers for control of vertical texture and magnetic anisotropy (Ta 3nm/Pd 4nm/ [Co 0.2 nm/ Pd 0.8 nm)]$_8$. The magnetic material on top of the Si pillars is closer to the recording head and thus predominantly dictates the recording behavior as the media material deposited in the valley will be far away to contribute significantly to the signals picked up by read head.

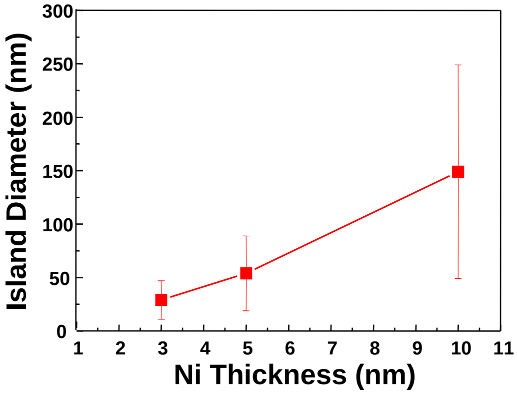

Fig. 14. Ni island diameter and distribution as a function of the initial Ni coating thickness.

The M-H magnetization loops were measured by MOKE (magneto-optical Kerr effect) and AGM (alternating gradient magnetometer) techniques and the data are shown in Fig. 16. Magneto-optical Kerr effect measurement of magnetic M-H loop for the magnetic recording media $(CoPd)_8$ multilayer on Si pillar arrays fabricated using Ni islands as the etch mask. The MOKE measurements agree well with the AGM data, and show that the "Region A" from the continuous $(CoPd)_8$ film in the valley location contributes to the lower switching field, which is corelated to the lower coercive force ($H_c \sim 600$ Oe) due to the disrupted multilayer texture alignment while the "Region B" from the $(CoPd)_8$ islands on top of Si pillars contributes to the much higher coercive force ($H_c \sim$ up to 3000 Oe, distributed).

The processing specifics of Ni island ball-up approach will be altered to obtain various distributions of the magnetic switching fields to gain insight on the effect of nanostructure geometry on the magnetic switching behavior. The required R&D toward ultra-high-density hard disk memory involve not only the reduction of magnetic island size but various materials and island shape parameters including texture formation, interface seed layer control (such as Pd, Ta type material layers), and the selection/modification of magnetic recording material itself (e.g., $L1_0$ phase vs $(CoPd)_n$ multilayer structure), and coercivity mechanisms. The advantage of this processing approach is that a relatively large sample area can be obtained (e.g., 1 cm^2) so that the difficulty of trying to measure extremely small magnetic M-H loop signals below the resolution of SQUID magnetometer in e-beam fabricated, small are (e.g., 100 x 100 μm area) can be bypassed. Materials parameters and processing specifics (for example, vertical texturing and anisotropy, coercivity control, etc.) can be optimized with these easily-measurable samples until the e-beam or nano-imprinted samples with desired geometry and large area can be fabricated to allow studies of magnetic switching and memory characteristics.

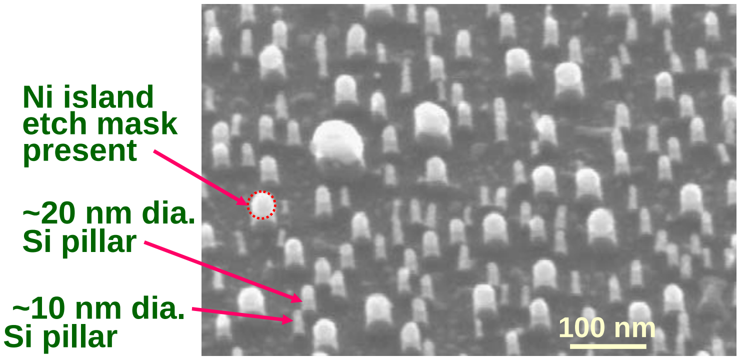

Fig. 15. SEM micrograph showing the Si pillars fabricated by RIE etching using Ni islands as the etch mask.

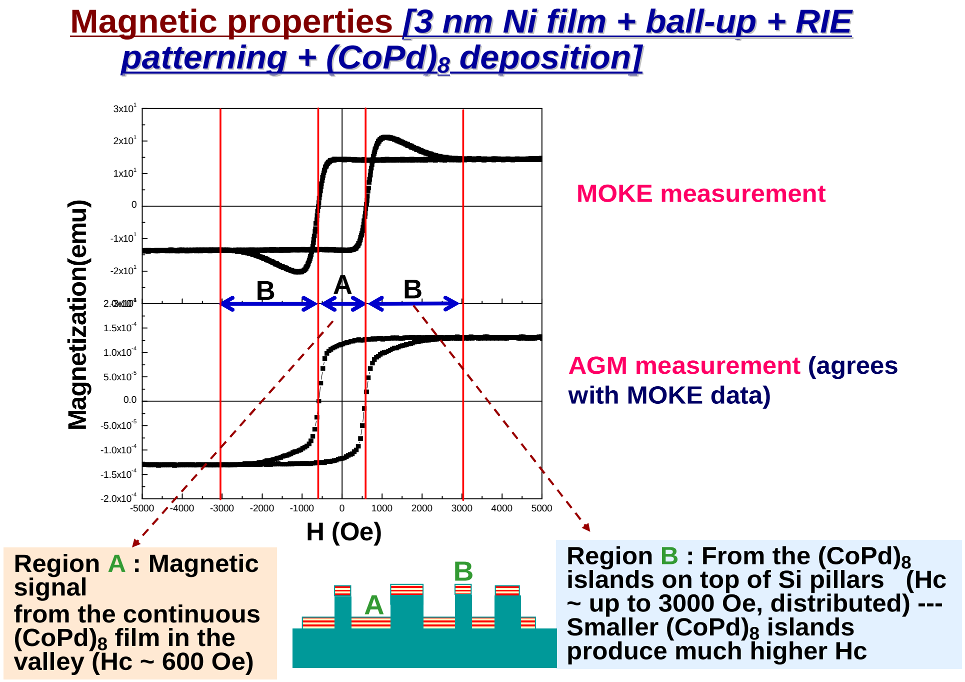

Magnetic properties *[3 nm Ni film + ball-up + RIE patterning + (CoPd)$_8$ deposition]*

Region A : Magnetic signal from the continuous (CoPd)$_8$ film in the valley (Hc ~ 600 Oe)

Region B : From the (CoPd)$_8$ islands on top of Si pillars (Hc ~ up to 3000 Oe, distributed) --- Smaller (CoPd)$_8$ islands produce much higher Hc

Fig. 16. Magneto-optical Kerr effect measurement of magnetic M-H loop for the magnetic recording media (CoPd)$_8$ multilayer on Si pillar arrays fabricated using Ni islands as the etch mask.

The Final Report

Title: Self-Assembled Liquid Crystalline Gels: From Nanostructure to Function.

Principal Investigator:

Professor Soo-Young Park, Kyung Pook University
Telephone: +82-53-950-5630
E-mail: psy@knu.ac.kr

Contract Number: FA4869-07-1-4071

AOARD Reference Number: AOARD-074071

AOARD Program Manager: Sang-ho Byun

Period of Performance: 1 year

Submission Date: 8 Oct 2008

Annual Progress Report

Caltech Part

Collaborative research between KNU and Caltech on new materials formed from block copolymers and small molecule liquid crystals (LC) during Year 1 of the AFOSR-MOST has included work at Caltech on:

- Synthesis of side-group liquid crystalline (SGLCP) polymers with systematically varied spacer length to guide the design of future block copolymers for increased response to stimuli
- Measurement of the effect of spacer length on the coil dimensions of polymers with fixed backbone length and fixed mesogenic group (varying only in the length of the spacer connecting each mesogen to the backbone).
- Developed and applied new methods to characterize the phase behavior of SGLCPs and small molecule LCs and the cooperative influence they have on each other's order
- Explored new means to create freely suspended LC films using LC-coil block copolymers to stabilize the free surface

These results and their relationship to our overarching goals are described below.

Synthesis of Homologous Series of Side Group Liquid Crystal Homopolymers.

Block copolymers with a side-group LC midblock and LC-phobic endblocks spontaneously form gels under conditions that cause the end-blocks to reject the solvent; this gelation is reversible, opening new opportunities for processing the materials. In contrast to *in-situ* polymerized networks, these physical gels are homogeneous systems. Consequently, the gels have exceptional clarity and their response to stimuli, such as change in temperature or electric field, is sharp—overcoming two of the major deficiencies of prior LC elastomers and gels. Our collaboration is addressing the need for structure-property relationships that connect the molecular structures of the polymer and LC solvent with the nanostructure that they spontaneously form, and between the nanostructure and macroscopic properties. One of the aspects of molecular design that is known to affect the electro-mechanical response of LC elastomers is the length of the flexible spacer that links mesogens to the backbone of the polymer[1]. During Year 1 we have synthesized a series of polymers that is uniquely suited to isolate the effect of spacer length, by holding other molecular parameters fixed (see Figure I). Specifically, all of the polymers in this homologous series of precisely matched backbone length and narrow distribution of chain length; and all of them have cyanobiphenyl mesogens.

We developed and optimized methods to synthesize mesogens with varying spacer lengths. Polymer analogous chemistry was used to attach the separately synthesized mesogenic side groups to polybutadiene backbones of known molecular weights, ensuring the major difference in the polymers was predominantly in the side-group spacer length.

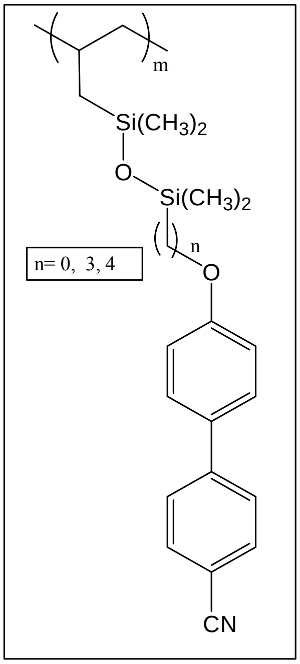

Figure I. The structure of our series of end-on side group liquid crystal polymers.

Effect of Spacer Length on Coil Dimensions

SGLCPs that adopt a more exapanded conformation in solution tend to undergo greater conformational change upon the transition between the isotropic and nematic phases; in turn, this correlates with a greater change in macroscopic dimensions of an elastomer or gel as a function of temperature or other stimuli. Therefore, the effect of spacer length on coil dimensions in solution is important to inform the design of SGLCP-coil block copolymers.

Small angle neutron scattering studies of our series of polymers in organic solvents of varying polarities, ranging from the very polar acetone to the less-polar toluene, has yielded interesting preliminary results. Figure II shows the polymers in mildly polar 1,1,2,2-tetrachloroethane ($\varepsilon_0 = 7$). Guinier analysis of the low q region suggests that the polymers with the longer spacers 104PBSiCB4 and 104PBSiCB3 (n=4 and 3, respectively) have the smallest radii of gyration, while the polymer with the smallest spacer, 107PBSiCB0 (n=0), appears to be the largest, not plateauing at all at low q.

We also discovered that the structure factor for the shortest spacer-polymer, 107PBSiCB0, appears markedly different than the other polymers (see Figure II). This polymer appears to be more extended than the other two, perhaps to accommodate having the bulky silane group closer to the mesogen. Backbone geometry can influence macroscopic properties such as viscoelasticity, transition temperature, and electrical and optical anisotropy[2], thus the ability to access differing backbone conformation lends us the ability to tailor macroscopic properties as needed for applications. In addition, we expect the backbone conformation to have significant affects on the solubility of the polymers in selective solvents.

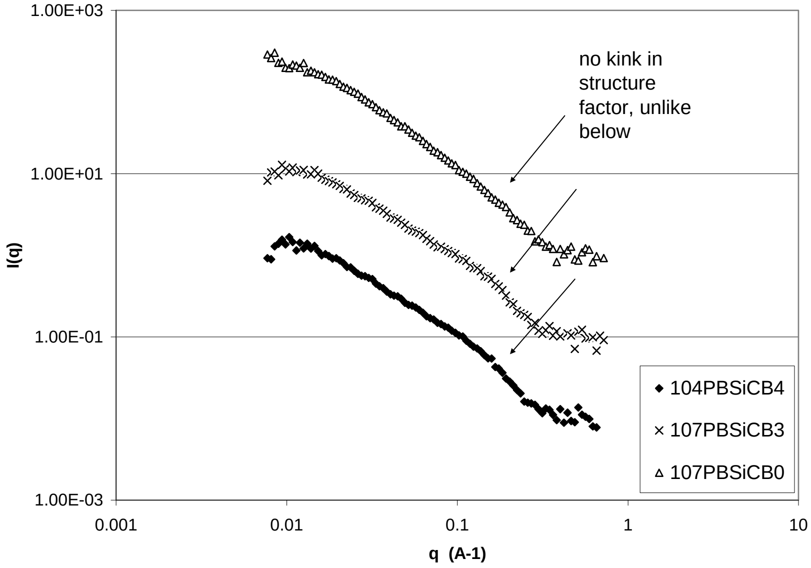

Figure II. Scattering patterns of polymers with different spacer lengths, n=0,3,4. Data was shifted by factors of 10 for visibility.

We also found that as we increased the polarity of the solvent, the polymers' radii of gyration all increased. Thus, we anticipate this difference to hold when the SGLCPs are dissolved in selective solvent, such as a small molecule liquid crystal, perhaps leading to noticeable differences in other macroscopic properties.

Thin Film Studies

Because so much of the proposed work centers on manipulating the phase behavior of diblock and tiriblock copolymer micelles, gels and networks, it is important to have a detailed and thorough understanding of the phase behavior of the side-group liquid crystal blocks in 4'-pentyl-4-cyanobiphenyl, 5CB, a small molecule liquid crystal.

Thin films of end-on and side-on SGLCP homopolymers were cast from organic solution and droplets of a small molecule liquid crystal, 4’-pentyl-4-cyanobiphenyl, 5CB were placed on the films. Polarized optical microscopy and quantitative FTIR measurements tracked the equilibration of these droplets over the course of 10 days.

In the case of the side-on SGLCP film, as the droplet spread over time, homeotropic alignment of 5CB was achieved (see Figure III), while end-on SGLCP film did not create the same affect. FTIR spectroscopy conducted in a lateral sweep suggests that the weight percent of side-on polymer varies very little across the droplet, though its birefringence obviously changes. This can be explained when one takes into account that the polymer backbone in a thin film is constrained to swell in fewer dimensions than bulk polymer. When liquid crystal is added on top of the polymer film, the polymer is thus constrained to swell mostly orthogonal to the surface it is mounted on (see Figure IV). The side groups of a side-on SGLCP run parallel to the backbone and are more likely to be oriented perpendicular to the surface, which in turn leads to a homeotropic alignment of the 5CB. This explanation also accounts for the fact that there no homeotropic alignment was observed when 5CB was spread over an end-on SGLCP film. If the mesogens are connected by their ends as opposed to their middles, stretching of the polymers backbones normal to the surface would orient the mesogens parallel to the surface, rather than perpendicular.

Figure III. Polarized optical microscopy conducted in a lateral sweep across the center of a 5CB droplet that is on a thin film of side-on SGLCP. The center of this droplet displays homeotropic anchoring.

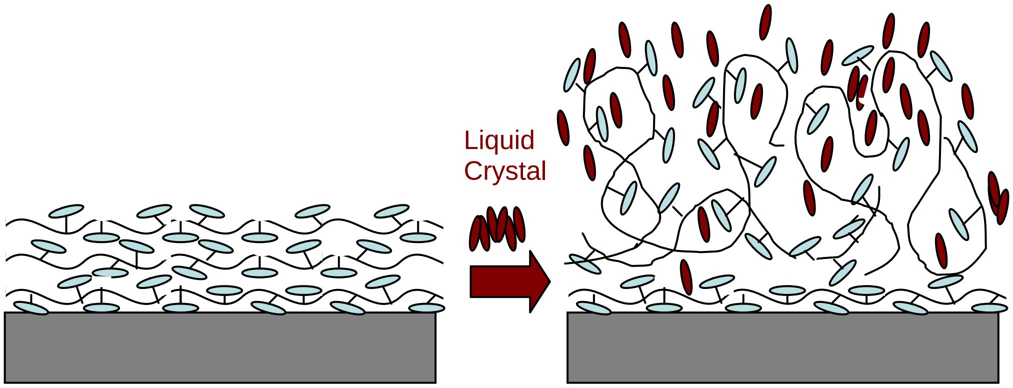

Figure IV. Schematic of side on SGLCP swelling in liquid crystal, resulting in a homeotropic orientation of the liquid crystal, depicted here as dark rods.

Quantitative FTIR measurements while heating the films past their nematic-isotropic phase transition temperature are also underway in order to construct a complete phase diagram of the system.

Future Work

Interactions at interfaces are of great interest in the development of chemical or biological sensors[3]. Liquid crystal ordering is sensitive to the microscopic structure at interfaces[4] and their ability to respond to changes in this environment makes liquid crystals ideal for sensors and actuators[5]. Abbott *et al.* has extensively studied the behavior at the liquid crystal-water interface, recently using surfactants to create emulsions and thus stabilized droplets of liquid crystal[6]. Using diblock block copolymers created by both the Caltech and the KNU teams, we propose the study of liquid crystal-air and liquid crystal-water interfaces. Analogous to surfactants, the non-liquid crystal blocks of our polymers can act as the agents driving the phase separation of the emulsions. These end-blocks can be tailored to the interface being studied, *i.e.* polystyrene for air, and polyphenylene vinylene for water. The self-assembly of the block copolymer at the interface may spontaneously create an anchoring condition, either parallel or perpendicular to the interface according to the molecular design (eg. end-on vs. side-on), similar to the anchoring in the thin films mentioned above (Figure III and IV).

Preliminary experiments studying the liquid crystal-air interface have been carried out by mounting films of diblock copolymer solutions on copper TEM grids by simply dipping them into the solution and suspending them in air. Figure V shows that even up to 10% polymer can be mounted on a TEM grid, where a polymer LC-film is present, the squares appear bright (birefringent) under crossed polars.

KNU Part

Summary;

In the 1st year, we prepared the PS-*b*-LCnP diblock and LCnP-*b*-PS-*b*-LCnP triblock copolymers using an ATRP (atomic transfer radical polymerization) method. For ATRP, we synthesized macroinitiators and ligands. Following are summary of the 1st year work

- Synthesis of LC monomers with various space lengths
- Polymerization of mono- and difunctioanl macroinitiators and synthesis of ligand and initiator for ATRP
- Polymerization of PS-*b*-LCnP diblock and LCnP-*b*-PS-*b*-LCnP triblock copolymers

1. Synthesis of LC monomers

LC monomers with a diphenyl group as the mesogen were synthesized. LC3, LC6 and LC11 are the LC monomers with three kinds of the spacer length to study influences of the space length on LC ordering. These monomers were confirmed by H^1-NMR.

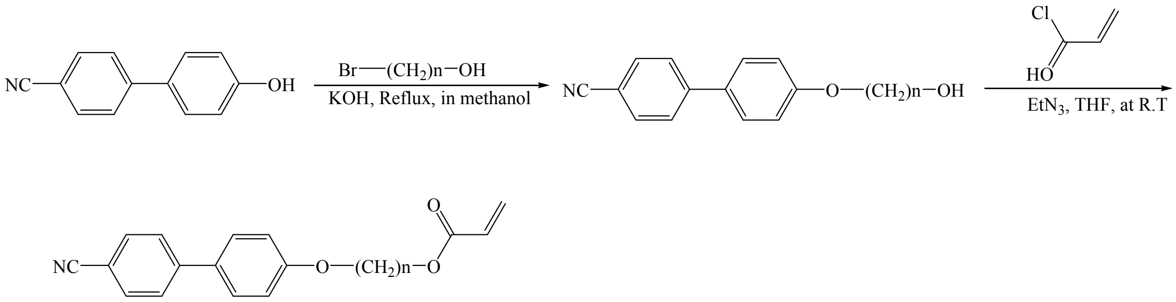

Scheme 1. Synthesis of LC monomers (n=3, 6, 11)

Synthesis of LC11 monomer. 4-hydrooxy-4'-cyanobuphenyl and potassium hydroxide were dissolved in 30mL of methanol at room temperature and the solution was brought to reflux before 1-bromo-1-undecanol in methanol was added. Chloroform (100ml) and water were added to the reaction mixture at the end of reaction followed by extractions with chloroform, and the crude product was collected by evaporating the solvent under reduced pressure after drying over anhydrous Na_2SO_4. Following recrystallization from acetone, flash chromatography on silica gel was accomplished using a 10:1 DCM/methanol micture as the eluent. 4-[(hydroxyundecyl)oxy]-4'-cyanobiphenyl and triethylamine were dissolved in dry THF, to which a solution of acryloyl chloride in dry THF was added dropwise. To the reaction mixtures were added methylene chloride and water, and the organic layer was dried over anhydrous Na_2SO_4. The crude product was isolated by evaporating the solvent and then flash chromatographed on silica gel with methylene chloride as the eluent. Further purification was accomplished by recrystallization from methanol to yield shiny white crystals.

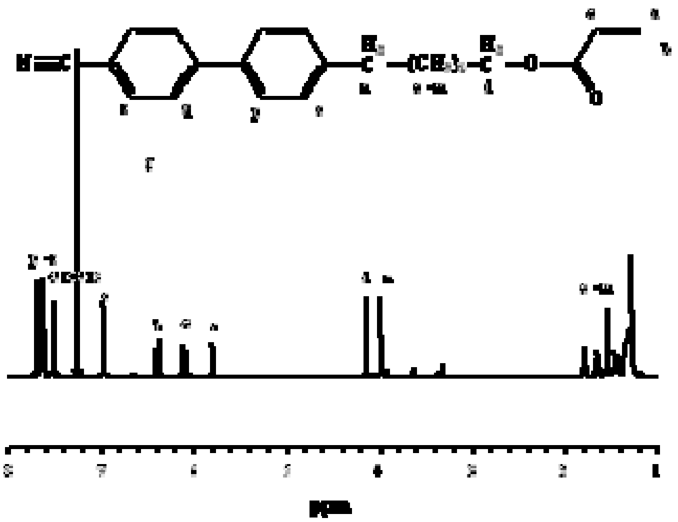

Figure 1. H^1-NMR spectra of LC11 monomer

Synthesis of LC6 monomoer. 4-[(Hydroxyhexyl)oxy]-4’-cyanobiphenyl was synthesized with the same method of LC 11 by changing 6-bromo-1-hexanol instead of 11-bromo-1-undecanol as a spacer.

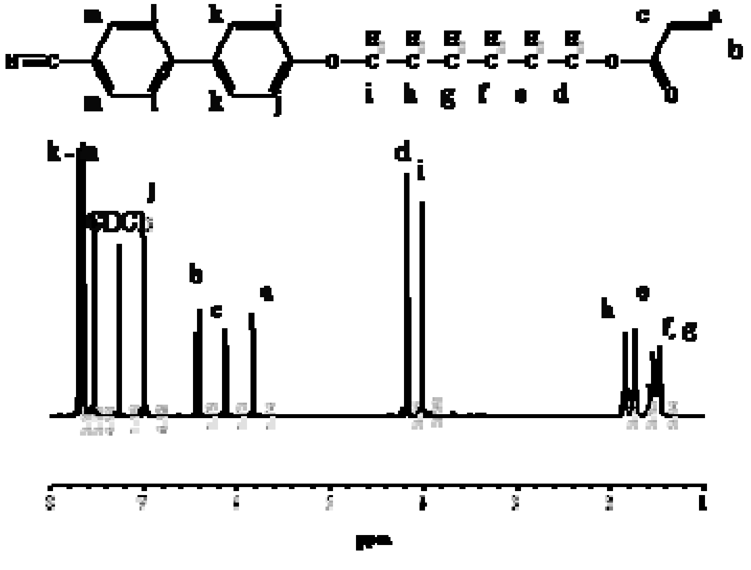

Figure 2. H^1-NMR spectra of LC6 monomer

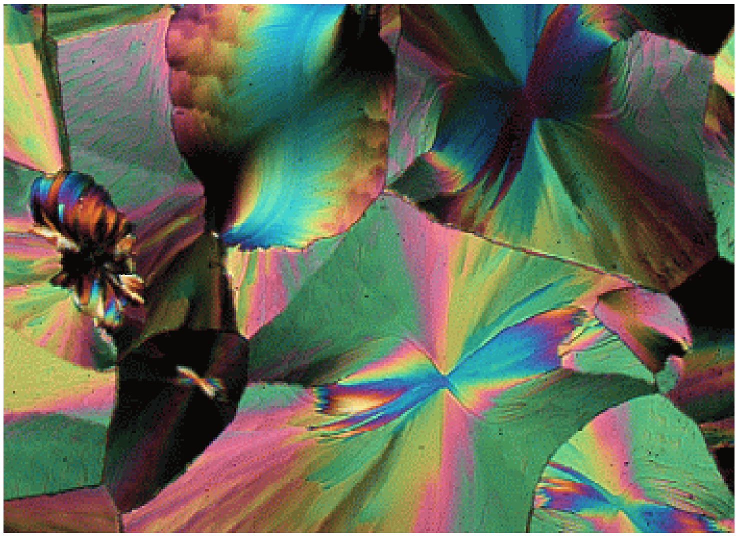

Figure 3. POM image of LC6 monomer (smectic phase)

Synthesis of LC3 monomoer. 4-[(Hydroxyundecyl)oxy]-4’-cyanobiphenyl was synthesized with the same method of LC11 monomer by changing 3-bromo-1-propanol instead of 11-bromo-1-undecanol as spacer.

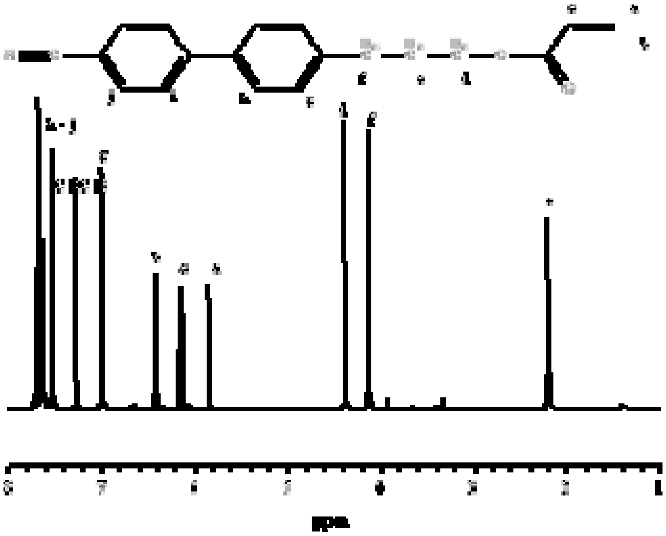

Figure 4. H^1-NMR spectrum of LC3 monomoer

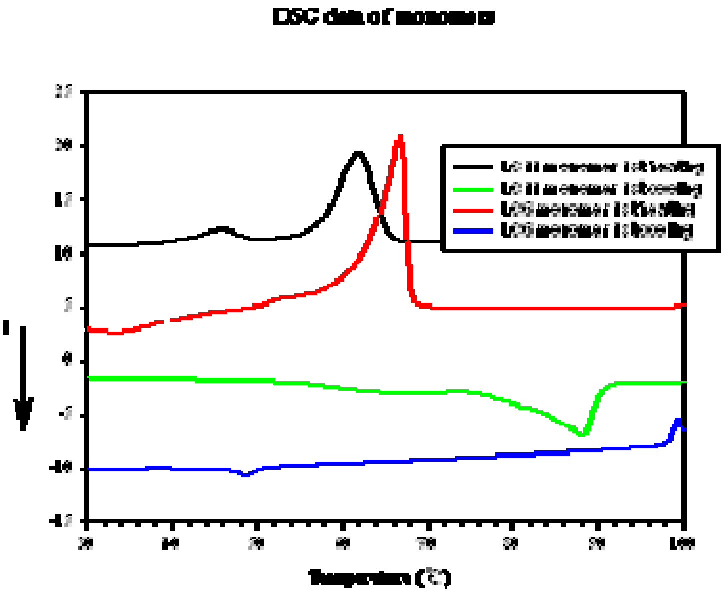

Figure 5. DSC data of LC6 and LC11 monomer

1-2. Polymerization of LC block copolymers

We have synthesized LC block copolymers with an ATRP(Atom Transfer Radical Polymerizaton) method. ATRP is more tolerant to moisture and trace amount of impurities as compared to anionic and cationic polymerizations. LC block copolymers were polymerized with PS-Br as macroinitiator, CuBr as catalyst and PMDETA as ligand. We used Me6TREN (which is stronger ligand than PMDETA) to polymerize diblock copolymers. Diblock copolymers were confirmed by H^1-NMR.

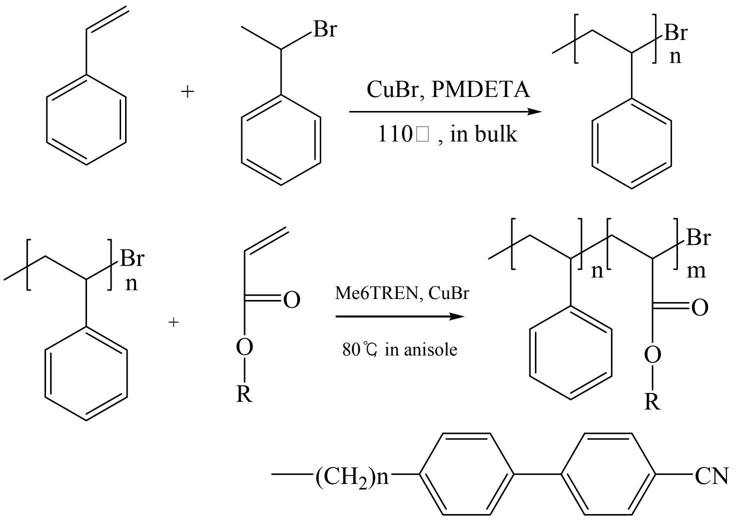

Scheme 2. Polymerization of PS-*b*-LCnP diblock copolymer

Polymerization of Macroinitiator

Polymerization of PS-Br(dPS-Br) macroinitiator by ATRP. CuBr and magnetic bar were added into a Schlenk flask. The flask was degassed by four vacuum-N_2 cycles. *N,N,N',N',N''*-pentamethyldiethylenetriamine (PMDETA), Styrene monomer and 1-phenyl ethyl bromide (1-PEBr) were previously degassed by bubbling N_2 through it for 30 min, were then introduced into the flask using a syringe purged with nitrogen. The flask was then placed in an oil bath thermostated at 110℃. After reasonable polymerization time, the resulting polymer solution was dissolved in THF, and passed through alumina column. After that it was concentrated by rotary evaporator and precipitated in methanol several times. The white polymer was dried under vacuum at 50℃ for 10hr.

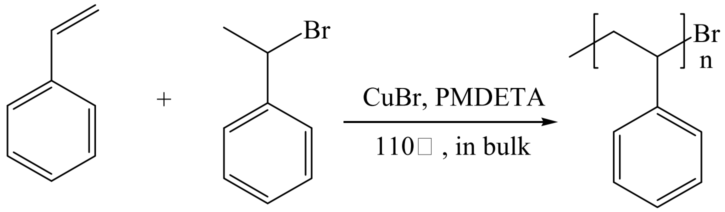

Scheme 3. Polymerization of PS-Br by ATRP

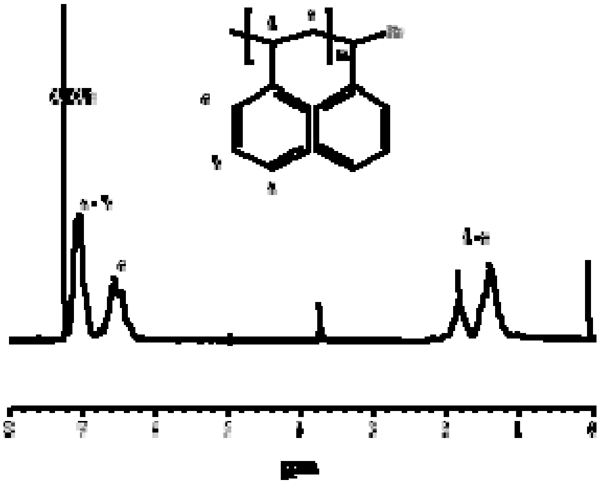

Figure 6. H^1-NMr spectrum of PS-Br macroinitiator

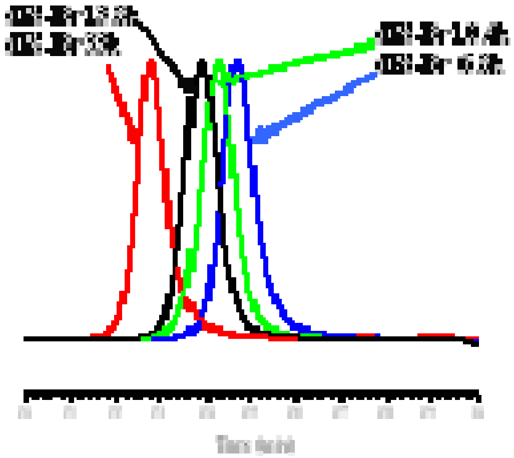

Figure 7. GPC data of PS-Br

Table. Molecular weights of PS-Br

Sample	**Mn**	**Mw**	**PDI (Mw/Mn)**
Ps-Br 6.8k	6000	6800	1.14
Ps-Br 10.4k	9200	10400	1.13
Ps-Br 13.8k	12300	13800	1.12
Ps-Br 33k	29200	33000	1.13

Synthesis of difunctional initiator; 1-Hydroxymethyl-1,1-di[(2-bromoisobutyrloxy)methyl] ethane was synthesized for a difunctioanl initiator to get Br-Ps-Br.

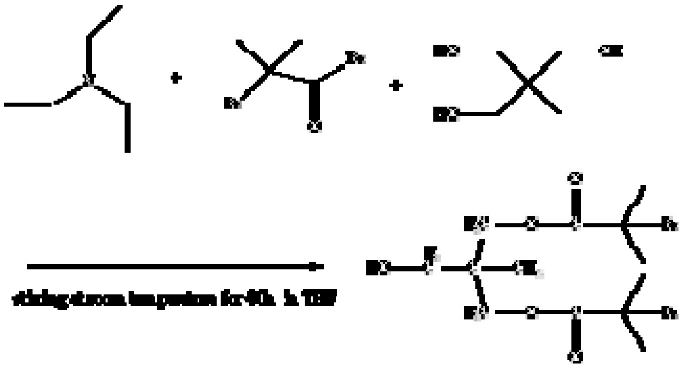

Scheme 4. Synthesis of 1-Hydroxymethyl-1,1-di[(2-bromoisobutyrloxy)methyl] ethane

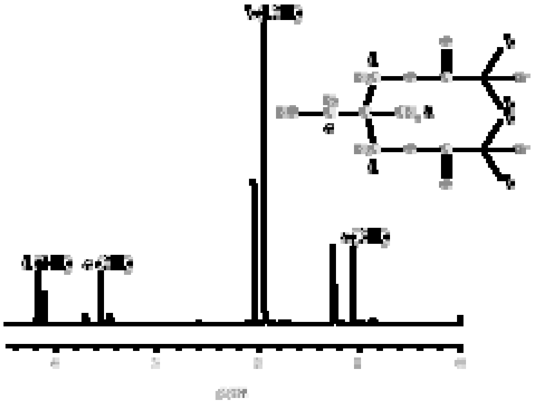

Figure 8. H^1-NMR spectrum of 1-Hydroxymethyl-1,1-di[(2-bromoisobutyrloxy)methyl] Ethane

Polymerization of Br-PS-Br(Br-dPS-Br) macroinitiator by ATRP. CuBr and magnetic bar were added into a Schlenk flask. The flask was degassed by four vacuum-N_2 cycles. *N,N,N',N',N''*-pentamethyldiethylenetriamine (PMDETA), Styrene monomer and 1-Hydroxymethyl-1,1-di[(2-bromoisobutyrloxy)methyl] Ethane as initiator were previously degassed by bubbling N_2 through it for 30 min, were then introduced into the flask using a syringe purged with nitrogen. The flask was then placed in an oil bath thermostated at 110℃. After reasonable polymerization time, the resulting polymer solution was dissolved in THF, and passed through alumina column. After that it was concentrated by rotary evaporator and precipitated in methanol several times. The white polymer was dried under vacuum at 50℃ for 10hr.

Synthesis of Ligand

Synthesis of Me6TREN; 3.0M HCl in methanol was added dropwise to tris(2-aminoethyl)amine in 50mL of methanol. After stirring at room temperature for 1hr, the precipitate was filtered and washed with methanol thrice. To prepare Me6TREN, (ClNH3CH2CH2)3NHCl, water, formic acid, and a formaldehyde aqueous solution were mixed. The mixture was heated under stirring in a 120℃ oil bath for 6hr, before volatile components were removed by rotary-evaporation. To the solid residue was then added 10wt% NaOH aqueous solution. After shaking, the aqueous phase was extracted with diethyl ether at 100mL each time for four times. The organic phase was combined, dried over anhydrous NaOH, and concentrated by rotary evaporation. After vacuum distillation at 62℃ and 133Pa, colorless oil was obtained.

Scheme 5. Synthesis of Me6TREN

Polymerization of homopolymer

Polymerization of LCnP homopolymer by ATRP. As outline in scheme 6, CuBr, LCn monomer and magnetic bar were added into a Schlenk flask. The flask was degassed by four vacuum-N_2 cycles. Me6TREN as ligand, and ethyl 2-bromoisobutyrate as initiator were previously degassed by bubbling N_2 through it for 30 min, were then introduced into the flask using a syringe purged with nitrogen. The flask was then placed in an oil bath thermostated at 80℃. After reasonable polymerization time, the resulting polymer solution was dissolved in THF, and passed through alumina column. After that it was concentrated by rotary evaporator and precipitated in methanol several times. The white polymer was dried under vacuum at 50℃ for 10hr.

Scheme 6 . Polymerization of LC homopolymer

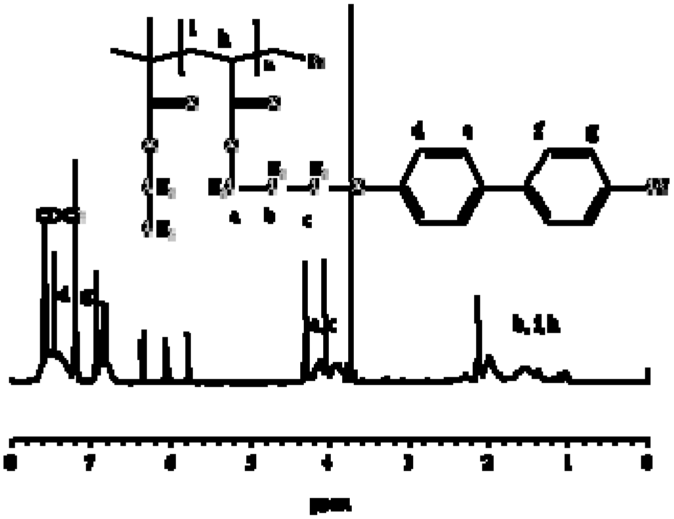

Figure 9. H^1-NMR spectrum of LC3 homopolymer (before removing monomer)

Polymerization of block copolymers

Polymerization of PS-*b*-LCnP diblock copolymer by ATRP. CuBr, LCn monomer, PS-Br macroinitiator and magnetic bar were added into a Schlenk flask. The flask was degassed by four vacuum-N_2 cycles. Me6TREN as ligand, and anisole as solvent were previously degassed by bubbling N_2 through it for 30 min, were then introduced into the flask using a syringe purged with nitrogen. The flask was then placed in an oil bath thermostated at 80℃. After reasonable polymerization time, the resulting polymer solution was dissolved in THF, and passed through alumina column. After that it was concentrated by rotary evaporator and precipitated in methanol several times. The white polymer was dried under vacuum at 50℃ for 10hr.

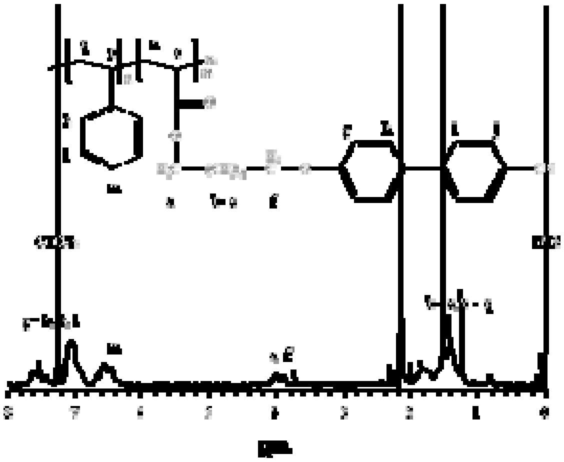

Figure 10. **H^1-NMR spectrum of PS-*b*-LC6P diblock copolymer (before removing monomer)**

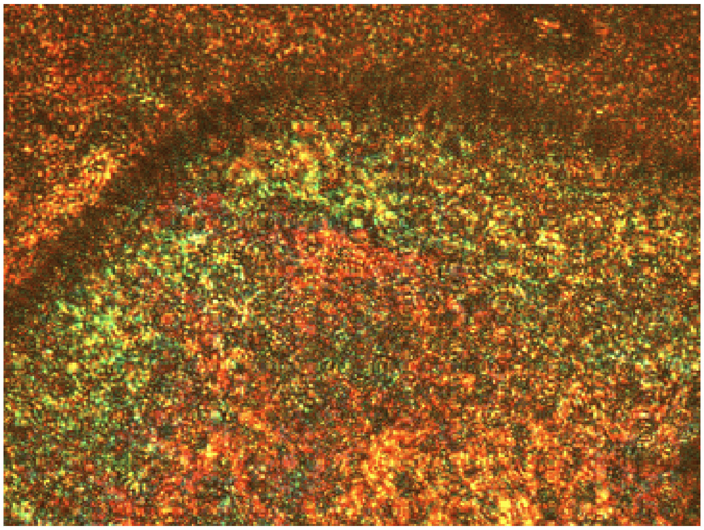

Figure 11. POM image of PS-*b*-LC6P

Polymerization of LCnP-*b*-PS-*b*-LCnP triblock block copolymers. CuBr, LCn monomer, Br-PS-Br macroinitiator and magnetic bar were added into a Schlenk flask. The flask was degassed by four vacuum-N_2 cycles. Me6TREN as ligand, and anisole as solvent were previously degassed by bubbling N_2 through it for 30 min, were then introduced into the flask using a syringe purged with nitrogen. The flask was then placed in an oil bath thermostated at 80℃. After reasonable polymerization time, the resulting polymer solution was dissolved in THF, and passed through alumina column. After that it was concentrated by rotary evaporator and precipitated in methanol several times. The white polymer was dried under vacuum at 50℃ for 10hr.

Future study

During the 1st year, we mainly focus on the synthesis of liquid crystal block copolymers using an ATRP method. We will apply these materials for micellar structure analysis (in 5 cb), phase diagram, and surface modification.

1. SANS study; we have tried to polymerize PS-*b*-LCnP diblock and LCnP-*b*-PS-*b*-LCnP triblock copolymers. the micellar structures in low molecular LC (5cb) were studied with this samples by using SAXS (small angle X-ray Scattering). However, there was no scattering due to small difference of electric densities between solvent and micelle. For the alternative method, SANS (small angle neutron scattering) was considered for analysis of the micellar structure in 5cb. For this purpose, deuterated macroinitiators were synthesized at CNMS (center for nanophase materials and science) of Oak Ridge National Lab.

2. Phase diagram study; the ternary blend systems of PS/ PS-*b*-LCnP/5cb (and PS/ LCnP-*b*-PS-*b*-LCnP /5cb will be explored to investigate the possibility for applying these blend systems to polymer dispersed liquid crystal. The block copolymer can act as surfactant to control of LC droplet size. The phase diagram is the basic study for this application

3. Surface modification of substrate; these materials can be applied for surface modification of the substrate. These block copolymers can be anchored on the substrate so that the surface can selectively modified for control the orientation of the low molecular liquid crystal (5cb). These surface modified substrate can be used for sensors, smart windows, liquid crystal display, etc.

---

[1] Y. Zhao, A.M. Jamieson, B.G Olsen et al., J. of Pol. Sci.: Part B: Polymer Physics **44** (2006).

[2] D.Gu, S.R. Smith, A.M. Jamieson, M. Lee, V. Percec, J.Phys II France **3** (1993).

[3] J.S. Park, C.H, Jang, M.L. Tingey, A.M. Lowe, N.L. Abbott, J. or Colloid and Interface Sciences **304** (2006).

[4] *ibid.*

[5] M.I. Kingsinger, B. Sun, N.L.Abbott, D.M.Lynn, Advanced Materials **19** (2007).

[6] E.Tjipto, K.D. Cadwell, J.F.Quinn, A.P.R. Johnston, N.L. Abbott, F.Caruso, Nanoletters **6** (2006)